Phonon Line Emission Revealed by Self-Assembly of Colloidal Nanoplatelets

Mickaël D. Tessier,[†] Louis Biadala,[†] Cécile Bouet,[†] Sandrine Ithurria,[†] Benjamin Abecassis,[‡] and Benoit Dubertret[†,*]

[†]Laboratoire de Physique et d'Etude des Matériaux, CNRS, Université Pierre et Marie Curie, ESPCI, 10 rue Vauquelin, 75005, Paris, France and [‡]Laboratoire de Physiques des Solides, Université Paris-Sud, CNRS, UMR 8502, 91405, Orsay, France

ABSTRACT

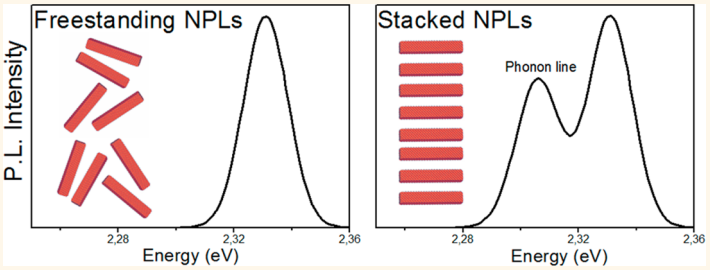

We show that colloidal nanoplatelets can self-assemble to form a 1D superlattice. When self-assembled, an additional emission line appears in the photoluminescence spectrum at low temperatures. This emission line is a collective effect, greatly enhanced when the NPLs are self-assembled. It is attributed to the longitudinal optical (LO) phonon replica of the band-edge exciton, and its presence in self-assembled nanoplatelets is explained using a model based on an efficient photons reabsorption between neighboring nanoplatelets. The presence of phonon replica at low temperatures in ensemble measurements suggests the possibility to design a laser, based on self-assembled nanoplatelets.

KEYWORDS: quantum well · self-assembling · collective properties · nanocrystals · photoluminescence · phonon · polaron

Colloidal semiconductor nanoparticles can now be synthesized with a very good control of their shape,[1−3] their size,[4,5] and their composition.[6] They have different physical properties compared to their bulk counterpart, that can be tuned thanks to a fine control of the morphology of the nanoparticles.[7] Just as nanoparticles have different properties than the bulk material, assemblies of nanoparticles can have collective properties that differ from those displayed by individual nanoparticles and bulk samples.[8] These new collective nanoparticle properties find their origin in several possible mechanisms. In the case of metallic nanoparticles, it can be the coupling of surface plasmons.[9] For example, when gold nanoparticles are placed sufficiently close to each other, near field coupling between the plasmons of individual nanoparticles results in spectral shift of the plasmons band as compared to the plasmon band of single nanoparticles.[10] For fluorescent semiconductor nanoparticles, the coupling of excitons can occur through Forster resonance energy transfer (FRET) as a result of dipole−dipole interactions between the nanoparticles when the interparticle distances are small (typically <10 nm).[11,12] Characteristic features of FRET include emission red shift, faster fluorescence lifetime of the donor, and reduced quantum yields.[13] It can be coupling of excitonic and plasmonic properties in hybrid metallic/semiconductor nanoparticles assemblies. Such coupling can lead to a strong Purcell effect,[14] fluorescence quenching or enhancement,[15,16] and absorption enhancement.[17] The plasmon-exciton interactions strongly depend on the mutual arrangement, the size, the shape, and the distance and the ratio between the metal and semiconductor nanoparticles. Finally, the coupling between nanoparticles can

* Address correspondence to benoit.dubertret@espci.fr.

Received for review January 8, 2013 and accepted March 2, 2013.

Published online March 03, 2013
10.1021/nn400833d

© 2013 American Chemical Society

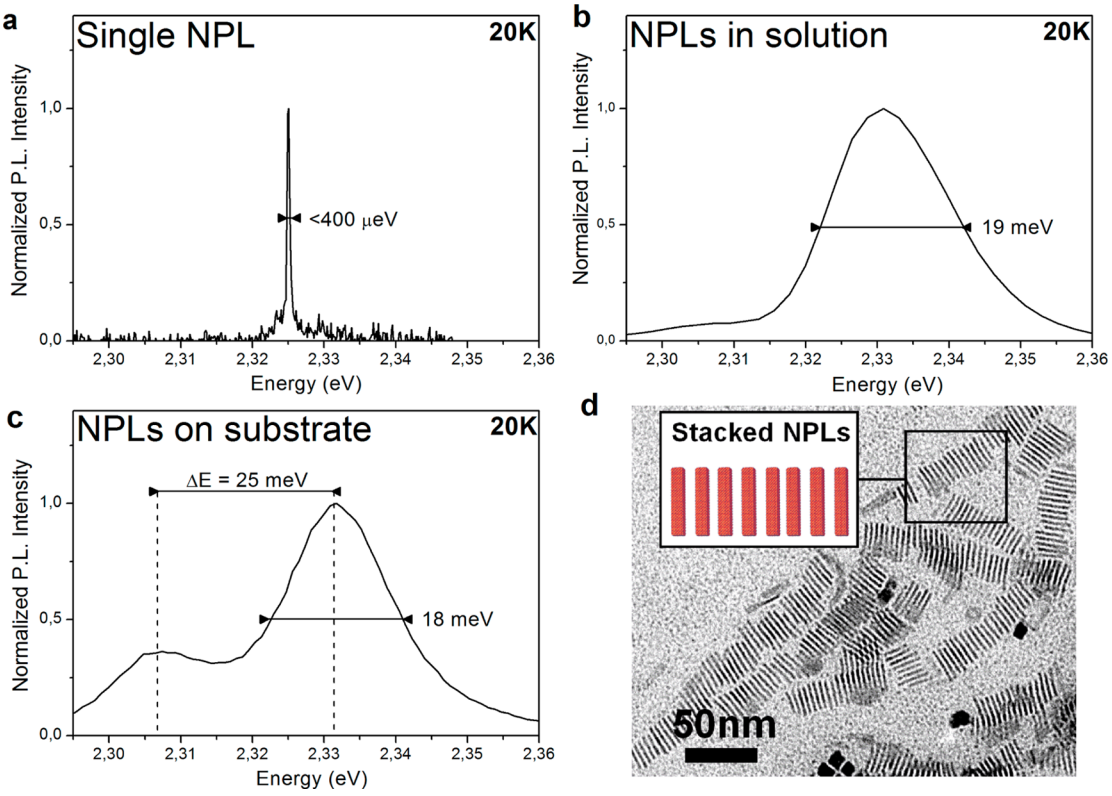

Figure 1. (a) PL spectrum of a single 553 NPL at 20 K; (b) PL spectrum of an ensemble of 553 NPLs in solution at 20 K; (c) PL spectrum of an ensemble of 553 NPLs drop-casted on a sapphire substrate at 20 K; (d) TEM picture of an ensemble of NPLs drop-casted on a TEM grid. Stacking of NPLs can be observed.

be due to magnetic coupling resulting from the dipolar interactions between magnetic nanoparticles.[18] Here, we study the modifications of the fluorescence emission of atomically flat semiconductor nanoplatelets (NPLs) induced by the nanoparticles self-assembly. NPLs are colloidal 2D nanoparticles with a thickness of few monolayers, controlled with atomic precision,[3] and lateral dimensions that can reach hundreds of nanometers. These NPLs are fluorescent, with an exciton that can be confined in one direction only, the NPL thickness, when the NPLs lateral dimensions are large compared to the exciton Bohr radius.[19] Their quantum yield can reach 50% at room temperature. Because the charge carriers in NPLs are confined in only one direction controlled with atomic precision, their emission spectra are extremely narrow with full width half-maximum (fwhm) close to $k \cdot T$ at room temperature, much more narrow than in the case of spherical[1] or rod shaped nanoparticles.[20] The NPLs have also a much shorter radiative fluorescence lifetime compared to nanoparticles with other shapes.[21] In this paper, we show that because of their anisotropic two-dimensional geometry, NPLs can self-organize into stacks to form a 1D superlattice. We demonstrate that such superstructures have different optical properties than single NPLs or than an ensemble of nonstacked NPLs. In particular, we show that the longitudinal optical (LO) phonon emission line of self-assembled NPLs is considerably amplified at cryogenic temperature compared to well dispersed NPLs. We propose a very simple model to explain this phonon line emission enhancement. The photoluminescence (PL) emission of self-assembled NPLs with three different thicknesses has been studied. These NPLs emit with emission maxima at 513, 553, and 576 nm respectively at room temperature. In the following, these NPLs populations will be referred as 513 NPLs, 553 NPLs and 576 NPLs.

RESULTS AND DISCUSSION

We have recently reported that, at room temperature, the emission spectrum of a single NPL is similar to an ensemble of NPLs.[22] This similarity is due to the absence of inhomogeneous broadening that is usually observed for spherical and rod-shaped particles and that is related to size variations. The fwhm of both a single NPL and an ensemble of NPLs are close to $k \cdot T$ at room temperature, and the dominant mechanism responsible for the fwhm is attributed to the exciton–phonon interactions. This interpretation is confirmed by the fact that the emission spectrum of an ensemble of NPLs is better fitted by a Lorentzian than by a Gaussian (Supporting Information, Figure S1). At 20 K, the emission fwhm of a single NPL becomes very narrow (<400 μeV, and resolution limited) at low excitation power (Figure 1a), but differs significantly from the PL spectrum of an ensemble of NPLs (Figure 1b). At 20 K,

an ensemble of unstacked NPLs displays PL emission spectrum with a fwhm close to 20 meV, much larger than a single NPL, and an emission profile that is better fitted with a Gaussian than with a Lorentzian (Supporting Information, Figure S2). We hypothesize that the large inhomogeneous broadening observed for an ensemble of unstacked NPLs at low temperature results from spectral diffusion.[23] Indeed, a single NPL observed for a long time (several minutes) displays spectral fluctuations that we hypothesized result from spectral diffusion. Similarly, when the excitation power increases, the fwhm of a single NPL becomes much larger and can reach a few meV.[22] In an ensemble of unstacked NPLs, it is very likely that local fluctuations of the environment result in different local charge fluctuations that yield to different emission maxima for each NPL. Thus they sum up in a Gaussian emission profile with large fwhm as observed in Figure 1b. The ensemble PL spectrum of stacked NPLs (Figure 1c) is different than the spectrum of unstacked NPLs at the same temperature. We observe the appearance of a second emission line 25 meV shifted to the low energy side of the main emission line. These two emission lines are better fitted by Gaussian than Lorentzian which suggests that the spectral diffusion is still the major source of broadening of the width of the two lines (Supporting Information, Figure S3). Before we analyze the origin of this new line, we rapidly discuss the NPLs stacking in Figure 1c.

The NPLs stacking is controlled with the solvent and the protocol used to prepare the NPLs for the measurement. In Figure 1b, the NPLs are suspended in 2,2,4-trimethylpentane before rapid cooling. In this case, the NPLs remain mostly unstacked even after cooling. In Figure 1c, the NPLs are suspended in hexane, and deposited by drop casting directly on a glass slide. In this case, the NPLs aggregate on the glass surface. NPLs aggregation on a TEM grid after solvent evaporation is shown Figure 1d. The NPLs stacking on a substrate was analyzed with small angle X-ray diffraction (Supporting Information, Figure S4). Two diffraction peaks corresponding to a stacking period of 5.1 nm are visible. The zinc-blende NPLs used in this manuscript have two large facets which end with atomically flat cadmium planes passivated with carboxylic acid ligands. The 5.6 nm distance corresponds to the NPL crystal thickness plus the inter NPL spacing induced by the ligands. These 553 NPLs are composed of five CdSe monolayers[24] which correspond to a thickness of ~1.5 nm if we neglect the possible lattice distortions induced by the ligands. The inter-NPLs distance is thus close to 4 nm, and results from the stacking of the long alkyl chains of the oleic acid ligands.

The appearance of the second low energy line at cryogenic temperatures in ensemble measurements when the NPLs are stacked is puzzling. The 25 meV energy difference between the emission maximum of the main line and the low energy line is very close to the energy of the LO phonon in bulk CdSe,[25] as well as in CdSe nanocrystals[26] and in tetrapods,[27] and it suggests that the low energy line could be the LO phonon line of the NPLs. However, several observations may apparently contradict this suggestion. First, this low energy line is not present at cryogenic temperatures when a single NPL is observed (Figure 1a), or in ensemble measurements when the NPLs are not stacked. The LO phonon line should be observed independently of the NPLs stacking, or of the number of NPLs observed. A second observation that led us to doubt about the phonon line interpretation is that the ratio of the integrated intensity between the main line and the low energy line fluctuates over more than an order of magnitude, depending on the region excited for a given sample, or from sample to sample (Supporting Information, Figure S5). Because of these contradictory observations, we have explored other hypotheses that could explain the appearance of the low energy line in ensemble measurements when the NPLs are stacked. First, the red-shifted line could result from the emission of defects in a sub population of NPLs. Second, one can think of some kind of excitons coupling between NPLs due to their close distance. Third, it could also be an intrinsic phenomenon such as biexciton[28−30] or trion generation[31,32] which is enhanced when NPLs stack. In the following, we test each of these hypotheses, and we show that none of them is correct. In the last section, we model the influence of the NPLs stacking on the NPLs emission and show that the apparent contradictions with the interpretation of the low energy line as a phonon line can be resolved. We conclude that the red-shift line that appears in the stacked NPLs emission is the CdSe LO phonon replica X^{LO} of the neutral exciton.

The PL emission of stacked NPLs is represented in Figure 2a for temperatures ranging from 300 to 20 K. It shows that the main emission line X^0, present at room temperature, is blue-shifted by 80 meV when the temperature decreases to 20 K. The red-shifted emission line that could not be detected at room temperature appears clearly at about 120 K. The energy difference ΔE between the two lines is constant with temperature. The energy shift of the main line can be fit with the relation introduced by Varshni:[33] $E(T) = E(T=0) - \alpha T^2/(T+\beta)$, where α and β are two constants. The experimental data are reproduced with $\alpha = (0.42 \pm 0.06)$ μeV·K^{-1} and $\beta = (180 \pm 60)$ K (Supporting Information, Figure S6). These values are similar to the values known in the literature for CdSe bulk,[34] dots,[35] rods, and tetrapods.[27] This confirms that X^0 is effectively the band edge emission line.

We then tested the hypothesis of the presence of a subpopulation of NPLs. The possibility that the two lines observed in Figure 1c stem from two different populations is tested spectroscopically with fluorescence

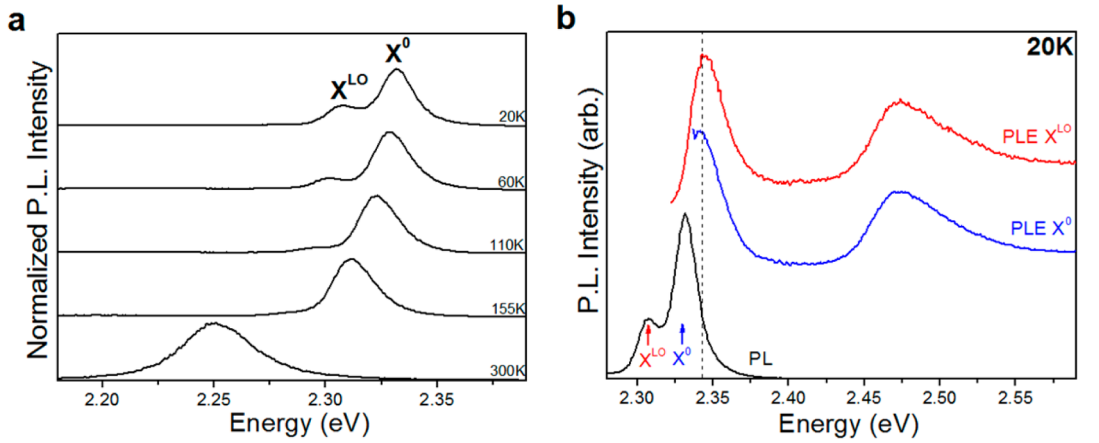

Figure 2. (a) Evolution with temperature of the photoluminescence spectrum of a film of NPLs. The sample is excited at 3.54 eV (350 nm) with a xenon lamp. The excitation power is the same at all temperatures (0.5mW/cm^2). Spectra have been shifted for clarity. (b) Photoluminescence (black) of the same film at 20 K. Corresponding excitation spectra at 2.31 eV (537 nm) in red and at 2.33 eV (532 nm) in blue. Spectra have been shifted for clarity.

excitation spectra (PLE) performed at low temperature both on the main emission line and on the red-shifted line (Figure 2b). The two lines have the same PLE spectrum which suggests that they are coming from the same NPLs population. The low energy line could also result from the emission of defects that would become visible at low temperature for a subpopulation of NPLs. We tested this hypothesis using fluorescence lifetime analysis of the two emission lines (Supporting Information, Figure S7). The main line and the red-shifted line have exactly the same fluorescence lifetime decay curve at 20 K with short lifetimes close to 300 ps. This rules out the possibility to have a defect-based emission for the red-shifted line since defects have longer fluorescence lifetimes than band edge recombinations.[36]

We then checked that the low energy additional line observed in Figure 1c was due to the NPLs stacking and not to other side effects such as coupling with the substrate, or drying of the NPLs. To address this point, we have developed a method to control the NPLs stacking in solution. The idea is to rapidly freeze the NPLs either in pure hexane, or in a solution containing a mixture of hexane and ethanol. To assess the structure of the dispersion at the nanometer scale and the stacking of the NPLs, we use synchrotron small angle X-ray scattering (SAXS).[37] In pure hexane, the NPLs are well dispersed and SAXS diagram of the solution displays a monotonous decay of the scattered intensity as a function of the scattering vector $|\mathbf{q}|$, characteristic of nanometric objects dispersed individually (Figure 3a, top). In contrast, when a small quantity of ethanol is added to the hexane solution, Bragg peaks appear in the scattering pattern of the solution (Figure 3b, top). These peaks appear at scattering vectors $|\mathbf{q}|$ values evenly spaced of $|\mathbf{q}^*|$, $|2\mathbf{q}^*|$, $|3\mathbf{q}^*|$ where $|\mathbf{q}^*| = 1.233\ \mathrm{nm}^{-1}$. This is characteristic of one dimension columnar assemblies of nanoparticles with an interparticle spacing of 3.6 nm. Hence, when ethanol is added to the dispersion, the NPLs stack one on top of each other. The addition of ethanol in the mixture leads to an increase of the polarity, which favor the self-assembly of NPLs in such a manner that their surface in contact with the solvent is minimized. Similar methods are used for size-selective precipitation of nanoparticles.[1] The solutions are then immersed in liquid nitrogen, and a PL emission spectrum is recorded in frozen hexane, or frozen ethanol+hexane. When the NPLs are dispersed in pure hexane, their emission spectrum displays a single peak (Figure 3a, bottom), slightly blue-shifted as expected for CdSe nanocrystals.[27,35] When they are dispersed in a mixture of hexane and ethanol (<10% of the volume of the solution), the NPLs emission spectrum clearly displays the low energy line (Figure 3b, bottom). These experiments prove that the low energy peak is directly connected with the stacking of the NPLs in solution.

The appearance of the low energy line for self-assembled NPLs could result from NPLs exciton–exciton coupling due to the small inter-NPLs distances. Such coupling should depend strongly on the inter-NPLs distance. We tested this hypothesis with ligand exchange on the NPLs that resulted in different NPLs interdistances after self-assembly. After a typical synthesis, the NPLs are capped with oleate ($C_{18}H_{33}OO^-$). To shorten the distance between the NPLs, the oleate, which has a theoretical length of ~2.5 nm,[38] was replaced by the shorter octanoate ligand ($C_8H_{15}OO^-$, theoretical length ~1 nm).[38] The exchange is confirmed by SAXS (Supporting Information, Figure S8) with Bragg peaks shifted toward higher wave vectors when the ligand is shortened. When the NPLs are coated with octanoate chains, the average distance between the NPLs after self-assembly is reduced by more than 30% to reach 3.8 nm. This important change of the inter-NPLs distance does not have an impact on

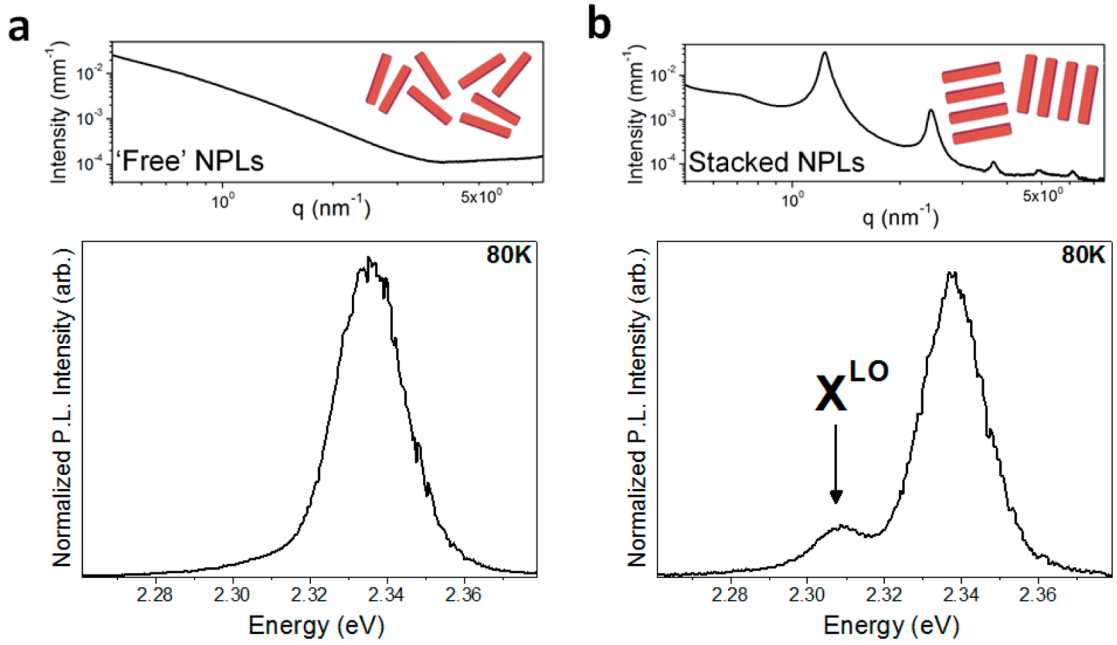

Figure 3. (a) NPLs in hexane solution. (Top) SAXS of the solution, stacking is not observed; (bottom) photoluminescence spectrum of the solution, the X^{LO} line is not observed. (b) NPLs in hexane after an addition of a small quantity of ethanol. (Top) SAXS of the solution, stacking is observed; the stack period is 5.1 nm. (Bottom) Photoluminescence spectrum of the solution. The X^{LO} line is observed.

photoluminescence properties, as the same red shift is observed for both ligands' lengths (Figure S8). This suggests that the two lines are not a consequence of inter-NPLs coupling. We also modified the chemical nature of the ligand. We replaced the carboxylate ligands by dodecanethiolate ($C_{12}H_{25}S^-$) ligands.[24] This change of ligands has a great impact on the excitonic structure of the NPLs since the nature of the chemical bond between the ligand and the NPLs surface is different. Indeed, a 130 meV redshift of the first exciton is observed after ligand exchange (Supporting Information, Figure S9). This redshift confirms the successful exchange as well as the quantum well barrier modification.[24] Despite this strong modification of the NPLs environment and of their excitonic structure, the red energy shift remains constant (Figure S9). This demonstrates that the ligand nature does not influence the magnitude of the energy shift ΔE. These experiments suggest that the low energy line is independent of the interactions between the exciton and the NPLs surface or their immediate environment. They also exclude the possibility of a charged exciton. Indeed, for CdSe/ZnS NCs, the negative trion state is red-shifted compared to the neutral state, but the shift can vary from 5 to 17 meV depending on the sample.[31,32] Such different values can be explained by different geometry or different dielectric environment of the nanocrystals. For NPLs, the energy shift is completely independent of these parameters.

The low energy line could also result from a biexciton emission. This hypothesis was tested with a power dependent excitation study of the NPLs spectra at

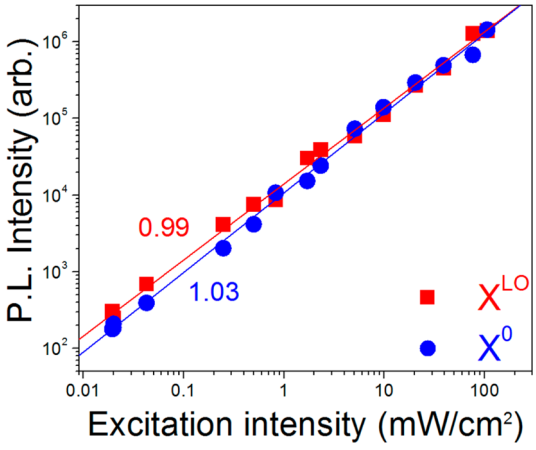

Figure 4. Integrated intensities evolution with the excitation power of the high energy line (blue) and the low energy line (red) in a log−log scale. Both lines can be perfectly fit with a linear growth.

cryogenic temperature. In Figure 4, we have represented the excitation intensity dependence on the integrated intensity of the two emission lines. Both lines display a perfect linear dependence over 5 orders of magnitude. This behavior excludes any biexcitonic origin of the low energy line, in which case the evolution would be quadratic.[28,39]

Since none of the hypotheses presented above could be validated, we tested more carefully the hypothesis that the red-shifted energy line could be the CdSe LO phonon line, as suggested by the ΔE = 25 meV energy shift. This energy shift was found to be independent of the NPLs surface ligands for the ligands

TABLE 1. ΔE Measured for NPLs with Different Ligands

	oleate	octanoate	dodecanethiolate
ΔE (meV)	25 ± 1	25 ± 1	25 ± 2

TABLE 2. ΔE Measured for NPLs with Different Lateral Sizes

	80 (nm^2)	125 (nm^2)	150 (nm^2)	190 (nm^2)	280 (nm^2)
ΔE (meV)	25 ± 1	25 ± 1	25 ± 1	25 ± 1	25 ± 1

TABLE 3. ΔE Measured for NPLs with Different Thicknesses

	513 NPLs	553 NPLs	576 NPLs
ΔE (meV)	25 ± 1	25 ± 1	26 ± 2

tested (Table 1), independent of the NPLs lateral dimensions for all lateral extensions tested (Table 2), and independent of the NPLs thickness (Table 3, and Supporting Information, Figure S10).

We further tested the hypothesis of the phonon line with NPLs made of other materials. PL emission spectra of stacked CdTe NPLs with two different thicknesses also display a red-shifted emission line, in both cases 20 meV lower than the main line (Supporting Information, Figure S11). This value, significantly smaller than for the CdSe NPLs, is close to the LO phonon energy of bulk CdTe in literature (21 meV).[40] The identical fluorescence lifetimes measured for the two PL lines (Supporting Information, Figure S7) is in agreement with the phonon hypothesis. For example, in the case of GaN free-standing films,[41] or in the case of self-organized perovskite $(C_6H_5C_2H_4{-}NH_3)_2PbI_4$ layers,[42] identical fluorescence lifetimes have been observed for band edge relaxation as well as for its phonon replica.

Overall, these experiments suggest that the low energy PL emission is the LO phonon replica. But before we can conclude, the following questions remain: why can we clearly observe the phonon replica in self-assembled NPLs while it is not observed for unstacked NPLs at similar temperatures? And how can we explain the strong intensity ratio variations between the two lines within one sample, and from one sample to the other? In the following, we show that these observations are related to the reabsorption of the main transition by neighboring NPLs, an effect that is greatly enhanced upon NPLs stacking, while the photons of the red-shifted line are not (or only slightly) reabsorbed by neighboring NPLs. Let us consider the following model: we suppose that all NPLs are identical and that a NPL has a probability $P_{em}(X^0)$ to emit a photon in the main line (band edge transition), and a probability $P_{em}(X^{LO})$ to emit a photon in the phonon line. The photons emitted in the X^0 line can be efficiently absorbed by neighboring NPLs because the Stokes shift between the main line emission and the first absorption exciton is small. On the contrary, the photons emitted in the X^{LO} line are strongly Stokes shifted and are not (or only weakly) reabsorbed by neighboring NPLs (Supporting Information, Figure S12). At 20 K, $P_{em}(X^{LO})$ is probably too weak compared to $P_{em}(X^0)$ to allow the observation of the X^{LO} line when single NPL spectroscopy is performed, and none of the emitted X^0 photons can be reabsorbed in this case. On the other hand, when NPLs are stacked, photons emitted by the X^0 line can be efficiently reabsorbed by neighboring NPLs (Figure 5a). The reabsorption of the photons emitted by the band edge transition leads to a decrease of the high energy line intensity. In contrast, the photons emitted by the X^{LO} line are not reabsorbed even in the case of stacked NPLs. In the case of a single NPL, or with a sample of unstacked NPLs, the intensity ratio of the main line to the phonon line is simply $I(X^{LO})/I(X^0) = P_{em}(X^{LO})/P_{em}(X^0)$. When the NPLs are stacked, the probability P_{abs} that a photon of the X^0 line is reabsorbed by a neighboring NPL cannot be neglected and the intensity ratio becomes $I(X^{LO})/I(X^0) = P_{em}(X^{LO})/(P_{em}(X^0)\cdot(1 - P_{abs}(X^0))$ (see Supporting Information, Figure S13 for more details). In the case of stacked NPLs, the phonon emission line intensity is thus enhanced by a factor of $1/(1 - P_{abs}(X^0))$ compared to the main line intensity. When $P_{abs}(X^0)$ becomes close to 1, that is for extended NPLs closely stacked, the phonon line can become dominant compared to the band edge emission (Supporting Information, Figure S14). On the contrary, for stacked NPLs with small lateral dimensions, the band edge emission is dominant (Figure S14). According to our model, the intensity ratio of the two lines is independent of the NPLs quantum yield and depends solely on $P_{abs}(X^0)$. For stacked NPLs with the same interdistance between NPLs, we expect that $P_{abs}(X^0)$ rises with the NPLs area. In Figure 5b, the intensity ratio of the main line to the phonon line has been plotted for NPLs that have the same thickness, but different lateral extensions estimated from TEM pictures. The intensities ratio increases with the NPLs lateral extension, as expected. Our simple model explains why the phonon line emission is visible when the NPLs are stacked while it cannot be detected on single NPLs or when the NPLs are well dispersed. It also explains why the intensities ratio between the main line and the phonon line may vary within one sample because the degree of stacking depends on the studied region of the sample. $P_{abs}(X^0)$ should also depend on the optical path for the detection and the excitation, that is, on the NPLs film thickness and theoretically on the NPLs orientation. However, the various measurements we have performed strongly suggest that $P_{abs}(X^0)$ depends mainly on the manner NPLs stack, and on the NPLs geometrical factor in the stack such as NPLs lateral dimension and NPLs interdistance.

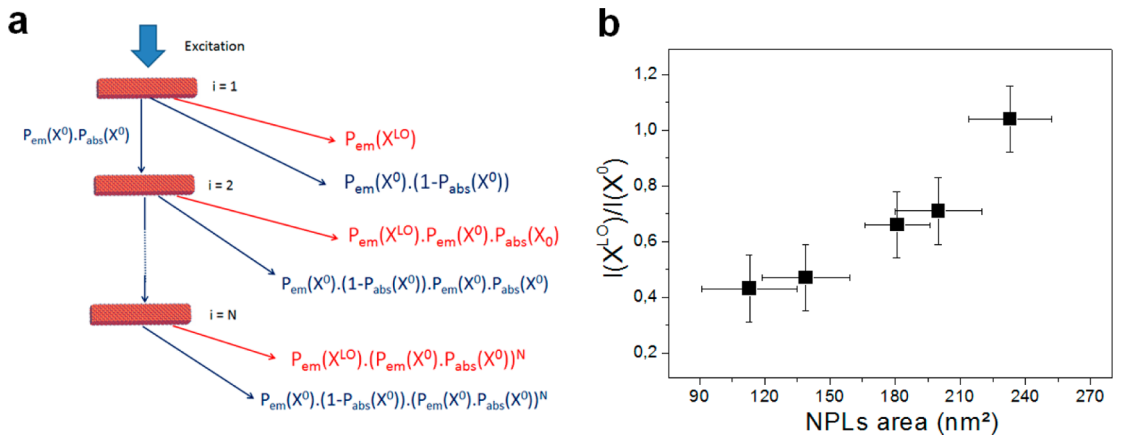

Figure 5. (a) Schematic model representing the possible paths for photon emitted in a stack of NPLs. In this model the probability for the X^{LO} line to be absorbed is zero, whereas the probability for the X^0 line to be absorbed is close to 1. (b) Experimental ratio of the X^{LO} line intensity to the X^0 line intensity *versus* the surface of the NPLs. The optical measurements have been made at 80 K in a solution of NPLs in which ethanol has been added to induce stacking. Average areas have been estimated statistically by measurement on transmission electron microscope images.

Comparatively, the other parameters such as film thickness or optical path are less important.

With the X^{LO} now clearly identified as an optical phonon line, we can also better understand the temperature dependence of the intensity ratio $I(X^{LO})/I(X^0)$ reported in Figure 2a. The disappearance of the X^{LO} line when the temperature increases could result from an enhanced absorption of the X^{LO} line with increasing temperature, a phenomenon that has been predicted on similar systems,[43] but that we have neglected in our simple model.

CONCLUSION

We have studied the PL spectra of ensemble of NPLs at cryogenic temperatures. We have shown that when the NPLs are not stacked, their emission spectra at cryogenic temperatures is broader than the one of a single NPL. When the NPLs self-assemble, a second red-shifted emission line is observed. We show that the energy difference between these two emission lines is independent of the NPLs size, thickness, and independent of the NPLs surface ligands. Intensity decay analysis shows that the two emission lines have the same fluorescence lifetimes, and power dependent excitation spectra rule out the possibility that the new line stems from multiexcitonic emission. The energy gap between these two lines is well-defined and depends only on the material (25 meV for CdSe and 20 meV for CdTe). We have attributed the high energy line to the band edge transition, and the low energy line to the phonon replica. A simple model based on reabsorption between NPLs explains the higher intensity of the phonon replica when the NPLs are self-assembled. Further investigations will aim at determining the evolution of the two lines at temperatures lower than 20 K. Besides its fundamental interest, we believe that this well-defined periodic structure formed by NPLs when they stack could have an interest. As this active medium filters the band edge emission, we can imagine confining the mode of the phonon replica in an optical microcavity to obtain lasing in an intrinsic exciton-polaron state.

MATERIALS AND METHODS

Chemicals. Cadmium nitrate dihydrate, cadmium acetate tetrahydrate $Cd(Ac)_2 \cdot 4H_2O$, technical grade 1-octadecene, myristic acid sodium salt, and selenium in powder were purchased from Sigma Aldrich. Methanol, ethanol, and hexane were purchased from VWR.

Synthesis of Cadmium Myristate. Cadmium nitrate (1.23 g) was dissolved in 40 mL of methanol. Then, 3.13 g of sodium myristate was dissolved in 250 mL of methanol (1 h with strong stirring). After complete dissolution, the two solutions were mixed. It gives a white precipitate. This precipitate was filtered and washed on a Buchner vacuum flask and dried under vacuum for about 12 h.

Synthesis of SeODE at 0.1 M. An amount of 140 mL of octadecene is degassed in a three-neck flask. Under argon flow, the temperature is set to 180 °C. A solution of 1.18 g of selenium dispersed in 10 mL of octadecene is slowly introduced into the hot octadecene until complete dissolution, while the temperature is increased from 180 to 205 °C. The solution is heated for 30 min at 205 °C.

Nanoplatelet Synthesis. *513 NPLs.* $Cd(myr)_2$ (170 mg, 0.3 mmol), 12 mg (0.15 mmol) of Se, and 15 mL of ODE were introduced in a three-neck flask and were degassed under vacuum. The mixture was heated up to 240 °C under argon flow. At 195 °C, 80 mg of $Cd(Ac)_2$ (0.30 mmol) were introduced. The mixture was heated for 10 min at 240 °C. At the end of the synthesis 0.5 mL of oleic acid was added to the solution. This synthesis produced 513 NPLs and also some QDs. The NPLs were separated from the QDs using selective precipitation. The NPLs were then dispersed in hexane.

553 NPLs. $Cd(myr)_2$ (170 mg, 0.3 mmol) and 14 mL of ODE were introduced in a three-neck flask and were degassed under vacuum. The mixture was heated under argon flow at 250 °C. A solution of 12 mg (0.15 mmol) of Se dispersed in 1 mL of ODE was quickly injected. One minute later, 120 mg of $Cd(Ac)_2$ (0.45 mmol) was introduced. The mixture was heated for 10 min

at 250 °C. At the end of the synthesis 0.5 mL of oleic acid was added to the solution. This synthesis produced 553 NPLs and also some QDs. The NPLs were separated from the QDs using selective precipitation. The NPLs were then dispersed in hexane.

576 NPLs. $Cd(myr)_2$ (170 mg, 0.3 mmol) and 13.5 mL of ODE were introduced in a three-neck flask and were degassed under vacuum. The mixture was heated under argon flow at 250 °C. A solution of 12 mg (0.15 mmol) of Se dispersed in 1.5 mL of SeODE was quickly injected. One minute later, 120 mg of $Cd(Ac)_2$ (0.45 mmol) was introduced. The mixture was heated for 10 min at 250 °C. At the end of the synthesis 0.5 mL of oleic acid was added to the solution. This synthesis produced several populations of NPLs. The 576 NPLs were separated from the others using selective precipitation. The NPLs were then dispersed in hexane.

Small Angle X-ray Scattering. SAXS experiments were performed at the SWING beamline of the SOLEIL synchrotron (Saint-Aubin, France). Platelet liquid dispersions were introduced in glass round capillaries and then flame-sealed. Measurements were carried out using a fixed energy of 12 keV and two sample-to-detector positions (1.07 and 6.56 m). The typical accessible range of scattering vector modulus **q** was 0.02−10 nm^{-1} ($q = 4\pi \sin\theta/\lambda$, where 2θ is the scattering angle and λ = 1.033 Å the wavelength). Scattering patterns were recorded on an AVIEX 170170 CCD camera formed by four detectors and radially averaged.

Optical Characterization of NPLs on Substrate. NPLs were drop-casted on a sapphire substrate. The NPLs concentration was low, with an optical density of <0.1 at wavelength of >350 nm. The sample was mounted in an Oxford optistat CF-V continuous flow cryostat where it was cooled by He vapor exchange gas. To reach a cryogenic temperature, the sample is subjected to a vacuum of less than 10^{-6} mbar. With this setup, the sample can be cooled to 10 K. Photoluminescence spectra and time-resolved fluorescence measurements over the temperature range 10−300 K were obtained using an Edinburgh FSP920 spectrometer. The sample was excited with an Edinburgh EPL375 laser diode with an emission wavelength at 376 nm or with a Xenon 450 W arc lamp at 350 nm. The detector used for the experiment is an Edinburgh Instrument S900MCP microchannel plate.

Optical Characterization of NPLs in Solution at 80 K. NPLs solutions were placed in a homemade cryostat. The NPLs concentration was low, with an optical density of <0.2 at wavelength >350 nm. This was performed using a UV visible spectrometer (Varian Cary 5E). The sample was cooled with liquid nitrogen. Photoluminescence spectra were obtained using a Fluoromax-3 Horiba Jobin Yvon spectrometer.

Conflict of Interest: The authors declare no competing financial interest.

Acknowledgment. We thank B. Mahler, B. Nadal, N. Lequeux, and T. Pons for stimulating discussions and advices. We are grateful to S. Pedetti for providing CdTe samples. We thank R. P. S. M. Lobo for the help for cryogenic experiments. We thank the Soleil Synchrotron (Saint-Aubin, France) for the award of beamtime 20110596 and Florian Meneau for local contact during the SAXS experiments. We are grateful to X. Xu for performing the TEM measurements. We thank R. Proux for helping in optical measurements. M. D. Tessier acknowledges the financial support of the University Pierre et Marie Curie. B. Dubertret acknowledges Agence Nationale de la Recherche for funding.

Supporting Information Available: Lorentzian and Gaussian curve fitting of PL spectra; small-angle X-ray diffraction of NPLs deposit on substrate; PL spectra on a sample using confocal microscope; Varshni curve fitting of the evolution of the maximum of emission of 553 NPLs; intensity decays at 20 K of ensemble of 553 NPLs; SAXS diagram and correlated PL spectra for different ligand coverage; PL spectra at 20 K for 513, 576 NPLs and CdTe NPLs; excitation and emission spectra at 20 K of 553 NPLs; scheme of the reabsorption model; PL spectra of NPLs on substrate for two different lateral extension. This material is available free of charge *via* the Internet at http://pubs.acs.org.

REFERENCES AND NOTES

1. Murray, C. B.; Norris, D. J.; Bawendi, M. G. Synthesis and Characterization of Nearly Monodisperse CdE (E = S, Se, Te) Semiconductor Nanocrystallites. *J. Am. Chem. Soc.* **1993**, *115*, 8706–8715.
2. Peng, X.; Manna, L.; Yang, W.; Wickham, J.; Scher, E.; Kadavanich, A.; Alivisatos, A. Shape Control of CdSe Nanocrystals. *Nature* **2000**, *404*, 59–61.
3. Ithurria, S.; Dubertret, B. Quasi 2D Colloidal CdSe Platelets with Thicknesses Controlled at the Atomic Level. *J. Am. Chem. Soc.* **2008**, *130*, 16504–16505.
4. Efros, A. L.; Efros, A. L. Interband Absorption of Light in a Semiconductor Sphere. *Sov. Phys. Semicond.* **1982**, *16*, 772–775.
5. Brus, L. E. A Simple Model for the Ionization Potential, Electron Affinity, and Aqueous Redox Potentials of Small Semiconductor Crystallites. *J. Chem. Phys.* **1983**, *79*, 5566–5571.
6. Michalet, X.; Pinaud, F. F.; Bentolila, L. A.; Tsay, J. M.; Doose, S.; Li, J. J.; Sundaresan, G.; Wu, A. M.; Gambhir, S. S.; Weiss, S. Quantum Dots for Live Cells, *in Vivo* Imaging, and Diagnostics. *Science* **2005**, *307*, 538–544.
7. Yin, Y.; Alivisatos, A. P. Colloidal Nanocrystal Synthesis and the Organic-Inorganic Interface. *Nature* **2005**, *437*, 664–670.
8. Nie, Z.; Petukhova, A.; Kumacheva, E. Properties and Emerging Applications of Self-Assembled Structures Made from Inorganic Nanoparticles. *Nat. Nanotechnol.* **2010**, *5*, 15–25.
9. Ghosh, S. K.; Pal, T. Interparticle Coupling Effect on the Surface Plasmon Resonance of Gold Nanoparticles: From Theory to Applications. *Chem. Rev.* **2007**, *107*, 4797–4862.
10. Su, K. H.; Wei, Q. H.; Zhang, X.; Mock, J. J.; Smith, D. R.; Schultz, S. Interparticle Coupling Effects on Plasmon Resonances of Nanogold Particles. *Nano Lett.* **2003**, *3*, 1087–1090.
11. Crooker, S. A.; Hollingsworth, J. A.; Tretiak, S.; Klimov, V. I. Spectrally Resolved Dynamics of Energy Transfer in Quantum-Dot Assemblies: Towards Engineered Energy Flows in Artificial Materials. *Phys. Rev. Lett.* **2002**, *89*, 186802.
12. Kagan, C.; Murray, C.; Bawendi, M. Long-Range Resonance Transfer of Electronic Excitations in Close-Packed CdSe Quantum-Dot Solids. *Phys. Rev. B* **1996**, *54*, 8633–8643.
13. Kagan, C.; Murray, C.; Nirmal, M.; Bawendi, M. Electronic Energy Transfer in CdSe Quantum Dot Solids. *Phys. Rev. Lett.* **1996**, *76*, 1517–1520.
14. Canneson, D.; Mallek-Zouari, I.; Buil, S.; Quélin, X.; Javaux, C.; Mahler, B.; Dubertret, B.; Hermier, J. P. Strong Purcell Effect Observed in Single Thick-Shell CdSe/CdS Nanocrystals Coupled to Localized Surface Plasmons. *Phys. Rev. B* **2011**, *84*, 1–6.
15. Shimizu, K. T.; Woo, W. K.; Fisher, B. R.; Eisler, H. J.; Bawendi, M. G. Surface-Enhanced Emission from Single Semiconductor Nanocrystals. *Phys. Rev. Lett.* **2002**, *89*, 117401.
16. Kulakovich, O.; Strekal, N.; Yaroshevich, A.; Maskevich, S.; Gaponenko, S.; Nabiev, I.; Woggon, U.; Artemyev, M. Enhanced Luminescence of CdSe Quantum Dots on Gold Colloids. *Nano Lett.* **2002**, *2*, 1449–1452.
17. Lee, J.-S.; Shevchenko, E. V; Talapin, D. V Au−PbS Core−Shell Nanocrystals: Plasmonic Absorption Enhancement and Electrical Doping *via* Intra-particle Charge Transfer. *J. Am. Chem. Soc.* **2008**, *130*, 9673–9675.
18. Pileni, M.-P. Self-assembly of Inorganic Nanocrystals: Fabrication and Collective Intrinsic Properties. *Acc. Chem. Res.* **2007**, *40*, 685–693.
19. Ithurria, S.; Bousquet, G.; Dubertret, B. Continuous Transition from 3D to 1D Confinement Observed during the Formation of CdSe Nanoplatelets. *J. Am. Chem. Soc.* **2011**, *133*, 3070–3077.
20. Manna, L.; Milliron, D. J.; Meisel, A.; Scher, E. C.; Alivisatos, A. P. Controlled Growth of Tetrapod-Branched Inorganic Nanocrystals. *Nat. Mater.* **2003**, *2*, 382–385.
21. Ithurria, S.; Tessier, M. D.; Mahler, B.; Lobo, R. P. S. M.; Dubertret, B.; Efros, A. L. Colloidal Nanoplatelets with Two-Dimensional Electronic Structure. *Nat. Mater.* **2011**, *10*, 936–941.

22. Tessier, M. D.; Javaux, C.; Maksimovic, I.; Loriette, V.; Dubertret, B. Spectroscopy of Single CdSe Nanoplatelets. *ACS Nano* **2012**, *6*, 6751–6758.
23. Empedocles, S. A. Quantum-Confined Stark Effect in Single CdSe Nanocrystallite Quantum Dots. *Science* **1997**, *278*, 2114–2117.
24. Mahler, B.; Nadal, B.; Bouet, C.; Patriarche, G.; Dubertret, B. Core/Shell Colloidal Semiconductor Nanoplatelets. *J. Am. Chem. Soc.* **2012**, *134*, 18591–18598.
25. Broser, I.; Broser, R.; Hoffmann, A. *Landolt-Bornstein Tables Vol.* 17; Springer-Verlag: Berlin, Germany; 1982; p 213.
26. Empedocles, S.; Norris, D.; Bawendi, M. Photoluminescence Spectroscopy of Single CdSe Nanocrystallite Quantum Dots. *Phys. Rev. Lett.* **1996**, *77*, 3873–3876.
27. Salman, A. Al; Tortschanoff, A.; Mohamed, M. B.; Tonti, D.; van Mourik, F.; Chergui, M. Temperature Effects on the Spectral Properties of Colloidal CdSe Nanodots, Nanorods, and Tetrapods. *Appl. Phys. Lett.* **2007**, *90*, 093104.
28. Louyer, Y.; Biadala, L.; Trebbia, J.-B.; Fernée, M. J.; Tamarat, P.; Lounis, B. Efficient Biexciton Emission in Elongated CdSe/ZnS Nanocrystals. *Nano Lett.* **2011**, *11*, 4370–4375.
29. Fisher, B.; Caruge, J.; Chan, Y.; Halpert, J.; Bawendi, M. Multiexciton Fluorescence from Semiconductor Nanocrystals. *Chem. Phys.* **2005**, *318*, 71–81.
30. Achermann, M.; Hollingsworth, J. A.; Klimov, V. I. Multiexcitons Confined within a Sub-excitonic Volume: Spectroscopic and Dynamical Signatures of Neutral and Charged Biexcitons in Ultrasmall Semiconductor Nanocrystals. *Phys. Rev. B* **2003**, *68*, 245302.
31. Louyer, Y.; Biadala, L.; Tamarat, P.; Lounis, B. Spectroscopy of Neutral and Charged Exciton States in Single CdSe/ZnS Nanocrystals. *Appl. Phys. Lett.* **2010**, *96*, 203111.
32. Fernée, M. J.; Littleton, B. N.; Rubinsztein-Dunlop, H. Detection of Bright Trion States Using the Fine Structure Emission of Single CdSe/ZnS Colloidal Quantum Dots. *ACS Nano* **2009**, *3*, 3762–3768.
33. Varshni, Y. P. Temperature Dependence of Energy Gap in Semiconductors. *Physica* **1967**, *34*, 149–154.
34. Hellwege, K. H. *Landolt-Börnstein: Numerical Data and Functional Relationship in Science and Technology*; Springer-Verlag, Berlin, Germany, **1982**.
35. Valerini, D.; Cretí, A.; Lomascolo, M.; Manna, L.; Cingolani, R.; Anni, M. Temperature Dependence of the Photoluminescence Properties of Colloidal CdSe/ZnS Core/Shell Quantum Dots Embedded in a Polystyrene Matrix. *Phys. Rev. B* **2005**, *71*, 1–6.
36. Baker, D. R.; Kamat, P. V Tuning the Emission of CdSe Quantum Dots by Controlled Trap Enhancement. *Langmuir* **2010**, *26*, 11272–11276.
37. Als-Nielsen, J.; McMorrow, D. *Elements of Modern X-ray Physics*, 2nd ed.; Wiley: Chichester, U.K., 2011.
38. Tanford, C. *Physical Chemistry of Macromolecules*; Wiley, New York, 1961; p 40.
39. Malko, A. V; Park, Y.-S.; Sampat, S.; Galland, C.; Vela, J.; Chen, Y.; Hollingsworth, J. a; Klimov, V. I.; Htoon, H. Pump-Intensity- and Shell-Thickness-Dependent Evolution of Photoluminescence Blinking in Individual Core/Shell CdSe/CdS Nanocrystals. *Nano Lett.* **2011**, *11*, 5213–5218.
40. Nimtz, G. *Landolt-Bornstein Tables Vol* 17; Springer-Verlag: Berlin, Germany, 1982; p 227.
41. Zhong, Y.; Wong, K. S.; Zhang, W.; Look, D. C. Radiative Recombination and Ultralong Exciton Photoluminescence Lifetime in GaN Freestanding Film *via* Two-Photon Excitation. *Appl. Phys. Lett.* **2006**, *89*, 022108.
42. Gauthron, K.; Lauret, J.-S.; Doyennette, L.; Lanty, G.; Choueiry, A. Al; Zhang, S. J.; Brehier, A.; Largeau, L.; Mauguin, O.; Bloch, J.; *et al*. Optical Spectroscopy of Two-Dimensional Layered (C(6)H(5)C(2)H(4)-NH(3))(2)-PbI(4) Perovskite. *Opt. Express* **2010**, *18*, 5912–5919.
43. Vasilevskiy, M. I.; Anda, E. V; Makler, S. S. Electron-Phonon Interaction Effects in Semiconductor Quantum Dots: A Non-perturbative Approach. *Phys. Rev. B* **2003**, *70*, 035318.